Modulation of Fermi velocities of Dirac electrons in single layer graphene by moiré superlattice

Q. Zou,[1,a)] B. D. Belle,[2,a)] L. Z. Zhang,[1,a)] W. D. Xiao,[1] K. Yang,[1] L. W. Liu,[1] G. Q. Wang,[1] X. M. Fei,[1] Y. Huang,[1] R. S. Ma,[1] Y. Lu,[3] P. H. Tan,[3] H. M. Guo,[1,b)] S. X. Du,[1] and H.-J. Gao[1,b)]
[1]*Institute of Physics, Chinese Academy of Sciences, Beijing 100190, China*
[2]*School of Physics & Astronomy, University of Manchester, Oxford Road, Manchester M13 9PL, United Kingdom*
[3]*Institute of Semiconductors, Chinese Academy of Sciences, Beijing 100083, China*

(Received 9 July 2013; accepted 24 July 2013; published online 11 September 2013)

Study of electronic properties of graphene on an anisotropic crystal substrate including boron nitride (BN) has raised significant interest recently due to the application of graphene based vertical hetero-devices. We have performed scanning tunneling microscopy (STM) and scanning tunneling spectroscopy studies of single-layer graphene on hexagonal BN (h-BN) substrates with an applied perpendicular magnetic field at low temperature. Different periodic moiré superlattices can be resolved with STM, and their quantized Landau levels in high magnetic field are investigated. The renormalized Fermi velocities of massless Dirac fermions in graphene are revealed to show dependent on the moiré superlattice. Density functional theory calculation verifies that the interlayer interaction between graphene and h-BN is stronger with smaller twisting angle between lattices of graphene and h-BN, thus, leading to a reduction in the velocity of charge carriers. Our results should provide valuable insight of electronic properties and device performance of graphene on crystal substrates. © *2013 AIP Publishing LLC*. [http://dx.doi.org/10.1063/1.4821178]

Graphene, a single-atom thick two-dimensional (2D) crystal of carbon atoms arranged in a honeycomb lattice, has been demonstrated for many applications,[1,2] owing to its myriad of properties and unique charge carrier behavior. In particular, its low energy quasi-particle charge follows linear dispersion $E = \hbar k V_F$ as if they were massless relativistic particles,[3–6] in which Fermi velocity (V_F) has information on a variety of fundamental properties and is found to be dependent on several factors. For example, Fermi velocities as high as 3×10^6 m/s can be achieved by modifying electron-electron interaction through electronic density change.[7] And angular resolved photon emission spectroscopy (ARPES) study has demonstrated that the V_F of graphene is inversely proportional to its dielectric constant when the environment is changed.[8] So far, most of these studies were performed on the macroscopic scale with manifestation of averaged properties of graphene layers, while the related microscopic study by using atomically resolved local probe techniques has been rare, but is extremely important for understanding its electronic nature. This becomes particularly important when the achievement of large-area single crystalline domain of graphene still remains great challenge: chemical vapor deposition (CVD) growth of graphene on metal coils/films or other insulating substrates often leads to multi-crystalline lattice.[9,10] Most of epitaxial growth of graphene on SiC (Ref. 11) and transition metal substrates (Cu,[12] Ir,[13,14] Pt,[15,16] etc.) also produces many domains with various orientations relative to the underlying crystal lattices. While micromechanical cleavage of graphite can provide single-crystalline graphene, subsequent transfer process onto the supporting substrate often causes structural imperfections of such as folds and wrinkles,[17] which inevitably leads to misorientations and multi-domains on substrate.

Recently, hexagonal boron nitride (h-BN) crystal has emerged as an excellent substrate for various graphene devices due to its atomically flat surface with wide band gap as compared with amorphous SiO_2.[18–21] Indeed, graphene on h-BN has demonstrated interesting physics, such as Hofstadter's butterfly,[22,23] fractional quantum hall effect,[24] Fermi velocity enhancement,[25] micrometer-scale ballistic transport,[26] and coulomb drag.[27] This type of vertical heterostructures provides great promising applications in future semiconductor industry.[20,28–30] The common approach for making graphene/h-BN devices relies on mechanical transfer as described above, with uncontrollable lattice misorientation of graphene with respect to the h-BN crystalline lattice (Fig. 1(a)). This inhomogeneous effect is typically ignored in most of current studies.

In this letter, we explore lattice orientation dependent Fermi velocities of Dirac electrons in graphene on h-BN crystal substrates by both experiment and theory. We have prepared single-layer graphene by micromechanical exfoliation from natural graphite and inspected it with micro-Raman spectroscopy to confirm a single-layer thickness (see the supporting information).[38] During the transfer process of graphene, the different lattice misorientation between graphene and h-BN can be naturally induced due to existence of such wrinkles (Fig. 1(b)). While some impurities and defects can be occasionally found on the graphene surface, scanning tunneling microscopy (STM) results presented below were always carried out in the areas away from wrinkles in order to avoid such as strain-induced effect. The STM/scanning tunneling spectroscopy (STS) experiments were conducted

[a)]Q. Zou, B. D. Belle, and L. Z. Zhang contributed equally to this work.
[b)]Electronic addresses: hmguo@iphy.ac.cn and hjgao@iphy.ac.cn

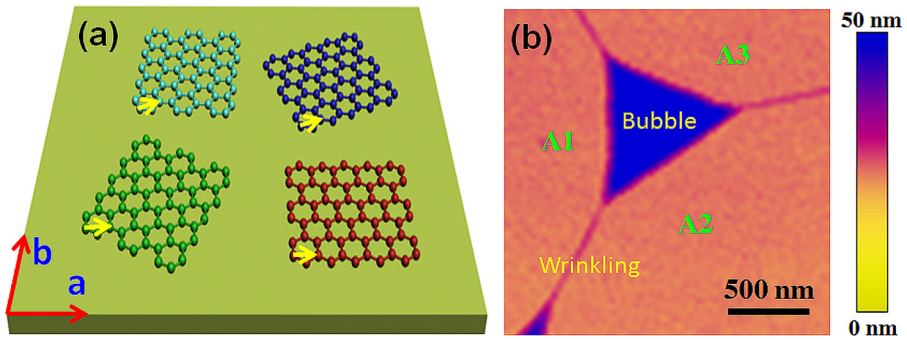

FIG. 1. Existence of mis-orientation between graphene and h-BN substrate. (a) Schematic of four single-layer graphene domains distributed randomly on h-BN crystal substrate with different twisting angles. The red and yellow arrows represent the direction of in-plane lattice vectors of h-BN substrate and graphene, respectively. (b) AFM image of graphene surface after dry-transfer onto h-BN substrate. A bubble and wrinkles can be seen and were formed during dry transfer process, with the average heights of about 45 nm and 4 nm, respectively. A1, A2, and A3 are three domains of graphene surrounding the bubble that possess could possess different twisting angles related to h-BN substrate.

with a UHV-LT-STM system (base pressure of 1×10^{-10} mbar, Unisoku) at 0.4 K using electrochemically etched W tips. Figure 2(a) shows schematics of STM measurement for the graphene device on h-BN substrate. A magnetic field up to 11 Tesla (T) is applied perpendicularly to the sample surface. Prior to STM/STS measurements, the graphene/h-BN sample was annealed at 260 °C in UHV for ~10 h to ensure surface cleanliness. The STM images were acquired in constant-current mode (all given voltages refer to the sample) and all differential conductance (dI/dV) spectra were measured using a lock-in technique with a 0.5 mV_{rms} sinusoidal modulation at a frequency of 973 Hz. Measurements of local spectroscopy were electronically calibrated by performing dI/dV measurements on clean Au(111) before and after measurements on graphene, based on the well-known Au(111) surface state.[31]

Figures 2(b) and 2(c) show topographic images acquired from two different areas of the single-layer graphene on h-BN. Both the atomic lattices of graphene and longer periodic hexagonal superstructures (moiré pattern) can be clearly revealed. The moiré pattern is formed by the interference between the graphene layer and underlying h-BN substrate, and can be attributed to their lattice mismatch ($a_{Gr} = 0.2456$ nm, $a_{BN} = 0.2496$ nm) and misalignment. Distinct from the highly corrugated graphene layers on amorphous SiO_2 substrates, the graphene on h-BN flake is extremely flat with a height modulation of about 0.07 nm, indicating a uniform interaction between graphene and h-BN surface. Due to tiny wrinkles and bubbles inevitably introduced during the transfer process of graphene onto h-BN, the rotation angles between graphene and h-BN lattices may be changed, leading to moiré patterns with different periodicities and orientations. The periodicity of moiré pattern presented in Figs. 2(a) and 2(b) is 1.01 ± 0.03 nm and 2.26 ± 0.05 nm, respectively. The twisted angle of graphene with respect to the h-BN lattice can be evaluated by

$$\theta = \mathrm{ArcCos}\left[1 - \frac{a^2b^2 - \lambda^2(b-a)^2}{2ab\lambda^2}\right],$$

where a is the graphene lattice constant, b is the h-BN lattice constant, and λ is the periodicity of the moiré pattern. Thus, the θ of Figs. 2(a) and 2(b) is found to be $(14.0 \pm 0.1)^\circ$ and $(6.2 \pm 0.1)^\circ$, respectively. Alternatively, the θ can be extracted by performing the fast Fourier transformation (FFT) analysis of the STM images, as shown in the inset of Fig. 2. The outside set of spots correspond to the reciprocal lattice of graphene, while the inner set of spots are assigned to that of the moiré pattern stemming from the rotation between the single-layer graphene and h-BN substrate. Consistent twisting angles can thus be obtained from the relation between reciprocal vectors $\mathbf{k}_{BN} = \mathbf{k}_{graphene} - \mathbf{k}_{moiré}$.[21]

To explore electronic structure of the single-layer graphene on h-BN, we measured and compared differential

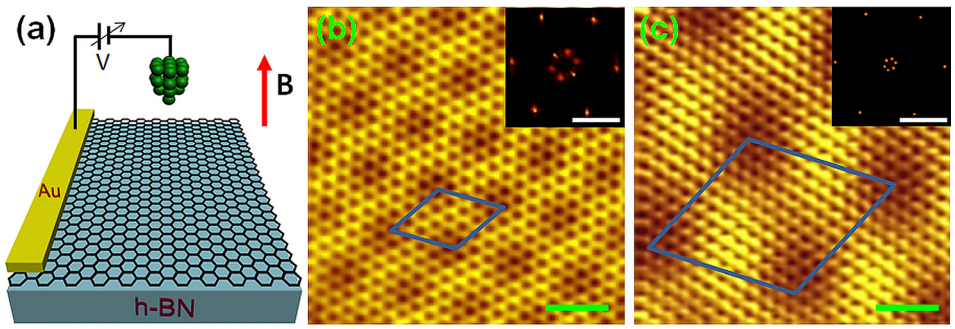

FIG. 2. STM characterization of a single layer graphene on a h-BN substrate. (a) STM/STS measurement schematics. (b) Topography of a moiré superlattice with periodicity of 1.01 nm and a 14.0° twist between graphene and h-BN. Image was acquired under condition of $V_b = -2.25$ V, $I_t = 10.0$ pA. (c) Topography of a moiré superlattice with periodical length of 2.26 nm and twist angle of 6.2°. Image was acquired under condition of $V_b = -2.00$ V, $I_t = 10.6$ pA. The scale bar is 1 nm. Blue rhombus in both images highlights unit cell of moiré superlattice. The insets of (b) and (c) are Fourier transform patterns of corresponding STM images with a scale bar of 2.56 $Å^{-1}$.

conductance (dI/dV) spectra under various magnetic fields in different Moiré superlattices. Figure 3(a) shows the dI/dV spectra with the magnetic field varying from 0 T to 10 T on the graphene area shown in Fig. 2(b) with a θ of 14.0°. A smooth V-shaped feature is observed in the absence of a magnetic field, showing that the intrinsic electronic structure of single-layer graphene is essentially preserved. A dip at −30 mV is observed in the dI/dV spectrum, demonstrating that the Dirac point is below the Fermi level, because of slight electron doping by the underlying h-BN substrate or charge impurities. A gap of ~78 meV at the Fermi level is attributed to the opening of an inelastic tunneling channel via the excitation of out-of-plane phonons, similar to the previous reports for graphene on SiO_2.[31]

At the presence of magnetic fields perpendicular to the graphene sheet, a series of peaks emerge at about 6 T. These sharp peaks can be assigned to the quantized Landau levels (LLs) due to the localization of the unusual quantum relativistic Dirac fermions of graphene in magnetic fields. At 9 and 10 T, the Landau index numbers are labeled in Figure 3(a). The intensities of these LLs and the intervals between them increase with increasing magnetic fields. The zero-mode LL could be found at −32 mV and stabilizes in all spectra acquired under different magnetic fields.

Same measurement performed in the region with θ of 6.2° shows similar features and LLs peak evolution at the presence of magnetic field, except that the LLs energies are different from those in Fig. 3(a). The zero mode LLs (Dirac point) are located at the Fermi level for θ of 6.2°. The variation of the Fermi level is due to a local effect of stochastic charge doping at these two moiré pattern areas.[18,21] Both Figs. 3(a) and 3(b) show the absence of LLs under low magnetic field. This observation can be attributed to the impurities adsorption and inhomogeneous carrier density caused by impurities doping.[32]

We have observed impurities and defects on graphene surface in both AFM and STM images, particularly in the areas close to such as wrinkles or Au electrodes (see the supplementary information).[38] It has been demonstrated that in electrical transport measurement such impurities and defects can act as the scattering centers and broaden LL, leading to an increase of the magnetic field required to clearly resolve the LLs.[33] In our current STM measurement, we intentionally performed measurement in defect free zones to avoid complications of results, and the tunneling spectroscopy method is applied to probe the local density of states (LDOS) and quantized LLs with atomic resolution (see images in Figs. 2(b) and 2(c)). As a result, those defects far away from measuring area do not contribute to as measured intrinsic landau levels, but they can scatter electrons tunneling into the LLs before transport to metal electrode (see Fig. 2(a) for STM measurement scheme), thus, suppressing the LLs signal in the STS at low magnetic field (see the supplementary information).[38] We have measured the dI/dV spectra of graphene at more than ten points in moiré unit cells far from the defects (above distance of 50 nm) for both regions of Figs. 2(b) and 2(c), and as-measured STS show consistent feature. The results demonstrate a high degree of uniformity spatially at flat areas on graphene/h-BN system.

Furthermore, the LLs of massless Dirac fermions of single-layer graphene can be given by[2]

$$E_n = E_D + \mathrm{sgn(n)} v_F \sqrt{2e\hbar B|n|},$$

where E_D is the energy of Dirac point, v_F is the Fermi velocity, e is the electron charge, $\hbar$ is the Planck's constant, B is the magnetic field, and n is the index of LLs. Fig. 3(c) summarizes and compares dependence of peak energies of the LLs for electron carriers on the reduced parameter $(B|n|)^{1/2}$ in both moiré superlattices. A linear relationship can be clearly revealed as theory predicted. Importantly, the Fermi velocity of massless Dirac fermions can be deduced from the slope of the linear fitting, and are found to be $(1.30 \pm 0.05) \times 10^6$ m/s and $(1.21 \pm 0.02) \times 10^6$ m/s in 14.0° and 6.2° regions, respectively.

The discovered modulation of Fermi velocity by the moiré superlattice is substantial. In order to gain insight into the geometric and electronic structures of the graphene/h-BN moiré superlattices, we carried out density functional theory (DFT) calculations with Vienna *ab-initio* simulation package (VASP).[34,35] The local-density approximation (LDA)[36,37] was employed, and the energy cutoff of the plane-wave basis

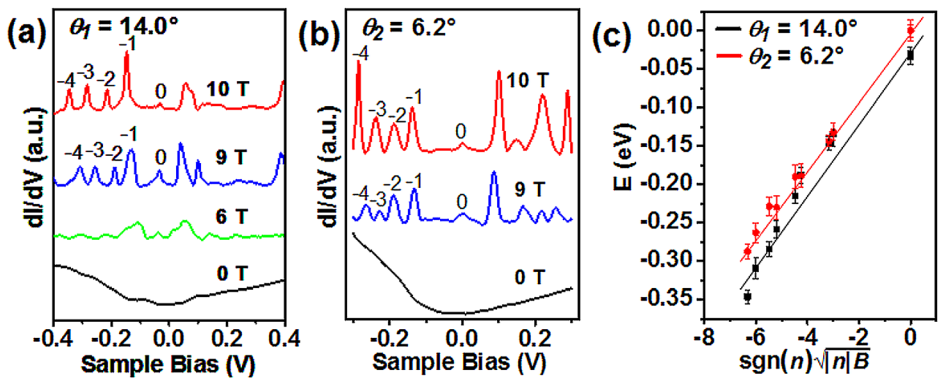

FIG. 3. Magnetic field dependence of differential conductance (dI/dV) spectra of graphene possessing different twisting angles related to the h-BN substrate at 0.4 K. (a) and (b) Differential conductance (dI/dV) spectra acquired from the two different moiré pattern regions on graphene in Figs. 2(b) and 2(c), respectively. The quantized LLs appear due to the localization of the quantum relativistic Dirac fermions of graphene under high magnetic fields. The curves are vertically offset for clarity. (c) Experimental and theoretical fitting of LLs energies vs. sgn(n) $\sqrt{B|n|}$. Linear fitting provides a way to evaluate Fermi velocity from STS measurement. The fitted Fermi velocities are 1.30×10^6 m/s and 1.21×10^6 m/s for graphene on h-BN substrates with twisted angles of 14.0° and 6.2°, respectively.

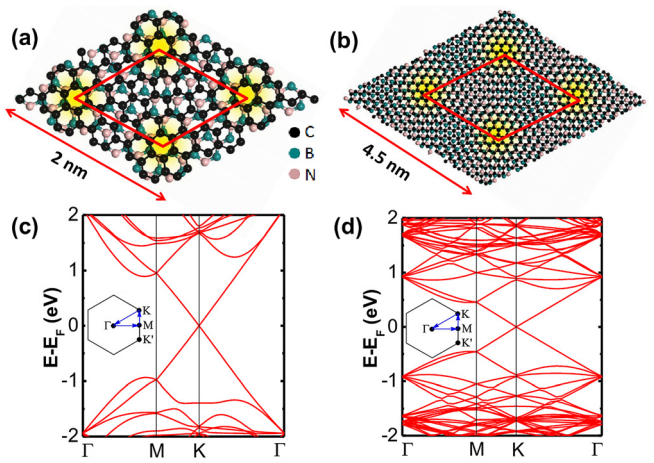

FIG. 4. Calculated band structures of graphene/h-BN with different twisting angles. (a) and (b) The top view of the relaxed graphene and h-BN layers in one supercell for the two moiré patterns (R14.0° model and R6.2° model). The black, pink, and blue balls are carbon, boron, and nitrogen atoms, respectively. (c) and (d) Calculated band structures for R14.0° model and R6.2° model indicate linear dispersion relationships near the Fermi level with the Dirac carrier velocities of 1.114×10^6 m/s and 1.055×10^6 m/s, respectively.

sets was 400 eV. The periodic slab model contains one layer h-BN, one layer graphene, and a vacuum layer of 15 Å. All atoms except the h-BN layer were fully relaxed until the net force on each atom was less than 0.01 eV/Å. Different K-point sampling were employed for Brillouin zone matrix integrations, where $5 \times 5 \times 1$ was used for the R14.0° model, and $3 \times 3 \times 1$ for the R6.2° model. Figures 4(a) and 4(b) show the top view of the relaxed graphene and h-BN layers in one supercell for the above two moiré patterns. The periodicity and the twisting angles are in agreement with the experimental results. Corrugations of carbon atoms in the graphene overlayer are very weak, i.e., 0.015 Å and 0.087 Å for R14.0° and R6.2°, respectively. The calculated band structures of these two models are presented in Figs. 4(c) and 4(d). Both of them exhibit line dispersion relationship near the Fermi level. The Fermi velocities of Dirac fermions can thus be obtained from the slopes for these two models, which are 1.114×10^6 m/s and 1.055×10^6 m/s for the R14.0° and R6.2° ones, respectively.

Based on DFT calculations, the calculated energy gap becomes much smaller (0.5 meV for R14.0° and 1.3 meV for R6.2°), which can be negligible even at low temperature, and the carriers can be still taken as massless Dirac Fermion. As shown by Xue *et al.*,[18] the interaction between graphene and h-BN can be analyzed similar to a twisted bilayer graphene system. Comparison between two moiré superlattices in Figs. 4(a) and 4(b) has revealed that when the two layers are superposed with relatively large twist angles, the interlayer hopping potential will decrease resulting from an increase in the average values of the distance between a carbon atom and a boron or nitrogen atom. This qualitatively explains the variations on the height corrugation and carrier velocity in graphene, i.e., a weakened interlayer coupling between graphene and h-BN with increasing twist angles.

In summary, we have discovered for modulation of Fermi velocity in different moiré superlattices due to the misorientations between graphene and single crystal h-BN substrates. By measuring magnetic field dependence of quantized LLS at the atomic scale, we have experimentally shown that the Fermi velocity of Dirac carriers in graphene is reduced as the periodicity of the moiré pattern is increased (i.e., larger misorientation). Our DFT calculation has further confirmed modulation of the electronic structure of graphene by the interlayer interaction from the underlying h-BN substrate with different twisted angles. This effect should be general for other crystalline substrates, in which moiré superlattice can be formed due to lattice mismatch. As a result, our finding has provided the microscopic insight of electronic structure of graphene, and should be important for understanding such as macroscopic transport measurements as well as development of emerging graphene based vertical hetero-devices.

The authors are grateful for A. K. Geim for helpful discussion and suggestion. Work at IOP was supported by grants from National Science Foundation of China (Nos. 61274011 and 51210003), National "973" projects of China (Nos. 2009CB929103, 2010CB923004, and 2011CB932700), the Chinese Academy of Sciences, and SSC. P.T. acknowledges the support from National "973" project (No. 2009CB929301) of China and NSFC Grant (No. 11225421). B.D.B. acknowledges the support from EPSRC of UK.

[1]A. K. Geim and K. S. Novoselov, Nature Mater. **6**, 183 (2007).
[2]A. H. Castro Neto, F. Guinea, N. M. R. Peres, K. S. Novoselov, and A. K. Geim, Rev. Mod. Phys. **81**, 109 (2009).
[3]K. S. Novoselov, A. K. Geim, S. V. Morozov, D. Jiang, M. I. Katsnelson, I. V. Grigorieva, S. V. Dubonos, and A. A. Firsov, Nature **438**, 197 (2005).
[4]Y. B. Zhang, Y. W. Tan, H. L. Stormer, and P. Kim, Nature **438**, 201 (2005).
[5]M. I. Katsnelson, K. S. Novoselov, and A. K. Geim, Nat. Phys. **2**, 620 (2006).
[6]A. F. Young and P. Kim, Nat. Phys. **5**, 222 (2009).
[7]D. C. Elias, R. V. Gorbachev, A. S. Mayorov, S. V. Morozov, A. A. Zhukov, P. Blake, L. A. Ponomarenko, I. V. Grigorieva, K. S. Novoselov, F. Guinea, and A. K. Geim, Nat. Phys. **7**, 701 (2011).
[8]C. Hwang, D. A. Siegel, S. K. Mo, W. Regan, A. Ismach, Y. G. Zhang, A. Zettl, and A. Lanzara, Sci. Rep. **2**, 590 (2012).
[9]X. S. Li, C. W. Magnuson, A. Venugopal, J. H. An, J. W. Suk, B. Y. Han, M. Borysiak, W. W. Cai, A. Velamakanni, Y. W. Zhu, L. F. Fu, E. M. Vogel, E. Voelkl, L. Colombo, and R. S. Ruoff, Nano Lett. **10**, 4328 (2010).
[10]J. Y. Chen, Y. G. Wen, Y. L. Guo, B. Wu, L. P. Huang, Y. Z. Xue, D. C. Geng, D. Wang, G. Yu, and Y. Q. Liu, J. Am. Chem. Soc. **133**, 17548 (2011).
[11]J. Hass, F. Varchon, J. E. Millan-Otoya, M. Sprinkle, N. Sharma, W. A. De Heer, C. Berger, P. N. First, L. Magaud, and E. H. Conrad, Phys. Rev. Lett. **100**, 125504 (2008).
[12]L. Gao, J. R. Guest, and N. P. Guisinger, Nano Lett. **10**, 3512 (2010).
[13]L. Meng, R. T. Wu, L. Z. Zhang, L. F. Li, S. X. Du, Y. L. Wang, and H. J. Gao, J. Phys.: Condens. Matter **24**, 314214 (2012).
[14]J. Coraux, A. T. N'Diaye, C. Busse, and T. Michely, Nano Lett. **8**, 565 (2008).
[15]M. Gao, Y. Pan, L. Huang, H. Hu, L. Z. Zhang, H. M. Guo, S. X. Du, and H. J. Gao, Appl. Phys. Lett. **98**, 033101 (2011).
[16]P. Sutter, J. T. Sadowski, and E. Sutter, Phys. Rev. B **80**, 245411 (2009).
[17]N. Liu, Z. H. Pan, L. Fu, C. H. Zhang, B. Y. Dai, and Z. F. Liu, Nano Res. **4**, 996 (2011).
[18]J. M. Xue, J. Sanchez-Yamagishi, D. Bulmash, P. Jacquod, A. Deshpande, K. Watanabe, T. Taniguchi, P. Jarillo-Herrero, and B. J. Leroy, Nature Mater. **10**, 282 (2011).
[19]C. R. Dean, A. F. Young, I. Meric, C. Lee, L. Wang, S. Sorgenfrei, K. Watanabe, T. Taniguchi, P. Kim, K. L. Shepard, and J. Hone, Nat. Nanotechnol. **5**, 722 (2010).

[20]L. Britnell, R. V. Gorbachev, R. Jalil, B. D. Belle, F. Schedin, A. Mishchenko, T. Georgiou, M. I. Katsnelson, L. Eaves, S. V. Morozov, N. M. R. Peres, J. Leist, A. K. Geim, K. S. Novoselov, and L. A. Ponomarenko, Science **335**, 947 (2012).
[21]R. Decker, Y. Wang, V. W. Brar, W. Regan, H. Z. Tsai, Q. Wu, W. Gannett, A. Zettl, and M. F. Crommie, Nano Lett. **11**, 2291 (2011).
[22]L. Wang, C. R. Dean, and P. Kim, Nature **497**, 598 (2013).
[23]R. V. Gorbachev, L. A. Ponomarenko, and A. K. Geim, Nature **497**, 594 (2013).
[24]C. R. Dean, A. F. Young, P. Cadden-Zimansky, L. Wang, H. Ren, K. Watanabe, T. Taniguchi, P. Kim, J. Hone, and K. L. Shepard, Nat. Phys. **7**, 693 (2011).
[25]J. S. Chae, S. Jung, A. F. Young, C. R. Dean, L. Wang, Y. D. Gao, K. Watanabe, T. Taniguchi, J. Hone, K. L. Shepard, P. Kim, N. B. Zhitenev, and J. A. Stroscio, Phys. Rev. Lett. **109**, 116802 (2012).
[26]A. S. Mayorov, R. V. Gorbachev, S. V. Morozov, L. Britnell, R. Jalil, L. A. Ponomarenko, P. Blake, K. S. Novoselov, K. Watanabe, T. Taniguchi, and A. K. Geim, Nano Lett. **11**, 2396 (2011).
[27]R. V. Gorbachev, A. K. Geim, M. I. Katsnelson, K. S. Novoselov, T. Tudorovskiy, I. V. Grigorieva, A. H. MacDonald, S. V. Morozov, K. Watanabe, T. Taniguchi, and L. A. Ponomarenko, Nat. Phys. **8**, 896 (2012).
[28]L. Meng, R. T. Wu, H. T. Zhou, G. Li, Y. Zhang, L. F. Li, Y. L. Wang, and H. J. Gao, Appl. Phys. Lett. **100**, 083101 (2012).
[29]M. P. Levendorf, C. J. Kim, L. Brown, P. Y. Huang, R. W. Havener, D. A. Muller, and J. Park, Nature **488**, 627 (2012).
[30]H. Wang, T. Taychatanapat, A. Hsu, K. Watanabe, T. Taniguchi, P. Jarillo-Herrero, and T. Palacios, IEEE Electron Device Lett. **32**, 1209 (2011).
[31]Y. B. Zhang, V. W. Brar, F. Wang, C. Girit, Y. Yayon, M. Panlasigui, A. Zettl, and M. F. Crommie, Nat. Phys. **4**, 627 (2008).
[32]Y. B. Zhang, V. W. Brar, C. Girit, A. Zettl, and M. F. Crommie, Nat. Phys. **5**, 722 (2009).
[33]T. Ando, A. B. Fowler, and F. Stern, Rev. Mod. Phys. **54**, 437 (1982).
[34]D. Vanderbilt, Phys. Rev. B **41**, 7892 (1990).
[35]G. Kresse and J. Furthmuller, Phys. Rev. B **54**, 11169 (1996).
[36]D. M. Ceperley and B. J. Alder, Phys. Rev. Lett. **45**, 566 (1980).
[37]G. Giovannetti, P. A. Khomyakov, G. Brocks, P. J. Kelly, and J. van den Brink, Phys. Rev. B **76**, 073103 (2007).
[38]See supplementary material at http://dx.doi.org/10.1063/1.4821178 for the fabrication process and Raman characterization of graphene devices, typical STM images of defects and impurities on graphene surface, as well as analysis of electron transport process in the STS measurement of graphene devices.